IEEE Access
Multidisciplinary | Rapid Review | Open Access Journal

Received 29 May 2024, accepted 17 June 2024, date of publication 20 June 2024, date of current version 28 June 2024.

Digital Object Identifier 10.1109/ACCESS.2024.3416950

RESEARCH ARTICLE

An Inertia Reserve Capacity Planning Method for Power Systems Considering Risk Preference

NA ZHANG[1], YONGRUI LI[2], QILI DING[3], (Student Member, IEEE), XINGGAN ZHANG[3], HAIWEI JIANG[1], AND WEIDONG LI[3], (Member, IEEE)

[1]State Grid Liaoning Economic Research Institute, Shenyang 110015, China
[2]State Grid Liaoning Electric Power Supply Company Ltd., Shenyang 110015, China
[3]School of Electrical Engineering, Dalian University of Technology, Dalian 116024, China

Corresponding author: Weidong Li (wdli@dlut.edu.cn)

This work was supported in part by the State Grid under Grant 2023YF-149.

ABSTRACT The traditional reserve planning method implicitly includes inertia in the frequency response reserve without realizing separate and accurate planning for inertia reserve, and cannot consider the risk preference of the decision maker, which leads to the homogenization of small probability extreme events. This paper refines the reserve classification system, adds inertia reserve for the first time, and proposes an inertia reserve capacity planning method considering the risk preference of decision makers. Based on the Sequential Monte Carlo method, component state models for conventional units, wind turbines, and photovoltaic units are established, and system load shedding sets are obtained through probabilistic production simulation. Based on the inertia response characteristics, the system frequency response model with multiple types of source-storage-load regulation resources is established to track the system frequency trajectory after disturbance. The minimum inertia demand is determined based on Rate of Change of Frequency (RoCoF) constraints, and then an inertia mismatch penalty model is constructed to measure the loss caused by RoCoF exceeding limits. The total cost-benefit model of inertia reserve considering risk preferences is then established, and the feasibility of the planning scheme is verified. Based on the improved IEEE RTS79 case studies, it is demonstrated that the proposed inertia reserve capacity planning method can flexibly formulate the optimal planning scheme under different risk ranges according to the decision maker's risk preferences and the grid's risk tolerance capability, avoiding the extreme events to be submerged in the massive and frequent occurrence of ordinary events, and effectively improving the risk response capability of the power system to extreme events, thus providing a more targeted decision basis for system planning, scheduling, and operation control.

INDEX TERMS Inertia response, reserve planning, inertia assessment, risk analysis, frequency stability.

I. INTRODUCTION

As the first defensive line for frequency stability control, inertia can provide power support quickly after system disturbance to gain time for subsequent governor action and other frequency control measures [1], [2]. Therefore, inertia is crucial for maintaining system frequency stability. With the accelerated development of new power systems, the proportion of inverter-based resources (IBR) such as wind power, photovoltaics, and energy storage is continuously increasing, and traditional synchronous generators are being replaced on a large scale, which makes the system synchronous inertia continue to decrease, and the power grid shows significant "low inertia" characteristics [3].

Low inertia will lead to deterioration of the RoCoF index, seriously threatening the safe and stable operation of the power grid [4]. For example, in the 2019 UK "8.9" major power outage, due to low system inertia, the RoCoF exceeded the relay protection setting value of the distributed generation, causing about 350 MW distributed generation out of the grid, which further exacerbated the degree of frequency drop, and ultimately caused a widespread power outage [5];

The associate editor coordinating the review of this manuscript and approving it for publication was R. K. Saket.

TABLE 1. Comparison of related work.

factor	Reference [22]	Reference [23]	Reference [24]	Reference [25]	This work
Risk analysis method	Global average risk analysis, which cannot consider the risk preferences of decision-makers.	VaR analysis method are insensitive to the risk value of extreme events.	Inability to continuously depict changes in decision makers' risk preferences	cVaR methods, insensitive to extreme risk values of inertia reserve	Using cVaR instruments, the extreme value-at-risk of inertia reserve can be measured
Reserve classification	Inertia is implicit in the frequency response reserve and unappreciated.	Inertia is implicit in the frequency response reserve and unappreciated.	Inertia is implicit in the frequency response reserve and unappreciated.	Inertia is implicit in the frequency response reserve and unappreciated.	Refinement of the reserve classification system for precise and separate planning of inertia reserve.
Effects of reserve	Focus on frequency nadir, unable to act quickly at the moment of disturbance	Focus on frequency nadir, unable to act quickly at the moment of disturbance	Focus on frequency nadir, unable to act quickly at the moment of disturbance	Focus on frequency nadir, unable to act quickly at the moment of disturbance	Focusing on mitigating RoCoF, able to act at the moment of disturbance.

In the 2016 South Australia "9.28" major power outage, due to the system inertia is too low, the RoCoF reached 6 Hz/s, causing the system frequency has collapsed before the under frequency load shedding action [6]. Insufficient inertia lead to frequent power grid accidents, causing enormous economic losses. Therefore, there is an urgent need to carry out theoretical research to safeguard the inertia of power grids.

To address this issues, related scholars have carried out research from multiple aspects. References [7], [8], and [9] make IBR have virtual inertia capability by designing inverter control strategy, which effectively make up for the lack of inertia caused by the integration of new energy units. References [10] and [11] propose wind-storage virtual inertia coordination support strategies and Photovoltaic-storage virtual inertia joint control strategies. References [12] and [13] evaluate and model the inertia response of induction machine, enriching the inertia resources on the load side. References [14] and [15] enhance the overall inertia level of the system by configuring virtual inertia. References [16] and [17] construct mathematical models for optimal power system day-ahead dispatch considering inertia security constraints, which guarantees grid inertia demand at the dispatch dimension. Reference [18] enables virtual power plants to provide inertia support capability through grid-forming inverters.

All the above studies have made rich achievements and provided theoretical guidance to guarantee the power grid inertia. However, there are fewer studies on inertia reserve planning at home and abroad. Under the traditional reserve classification structure, inertia is implied in frequency response reserve, without enough attention on inertia reserve. In the past, with the large proportion of synchronous units, the system rotational inertia is sufficient, and the reserve retention method naturally meets the inertia demand. With the continuous reduction of system synchronous inertia, the original rough reserve method will unable to meet the specific inertia demand of the system [19], it is necessary to carry out a more refined classification for reserve, and set up additional inertia reserve to guarantee the power grid inertia.

Currently, reserve planning methods mainly include deterministic methods, probabilistic methods, and risk decision methods. Deterministic and probabilistic methods are difficult to balance between economy and reliability, while risk decision methods can weigh between the two. With the continuous reduction of traditional synchronous inertia in the power grid and the emergence of virtual inertia resources, inertia response will no longer be a natural free response dominated by physical laws of traditional components [20], but will become an important part of auxiliary services in the power market [21]. Therefore, risk decision methods should be adopted for planning inertia reserve to balance the economy and reliability of the scheme.

On the other hand, the risk preference of grid decision-makers will affect the planning results. Traditional reserve planning methods based on the full incident set focus on average risk, which homogenizes the high-loss low-probability events with the low-loss high-probability events and fails to reflect the decision maker's risk preference, and leads to the extreme events being submerged in the huge number of frequently occurring common events [22]. Reference [23] employs the Value at Risk (VaR) analysis method for reserve planning, which, while considering the decision-makers' risk preferences, still discards some extreme events and is not sensitive to extreme risk values. Reference [24] does consider the risk values of high-risk, low-probability events, but it lacks the capability to continuously depict the impact of changes in the decision-makers' risk focus areas. Reference [25] uses conditional VaR (cVaR) analysis method for rapid frequency response reserve planning, which can continuously depict changes in the decision-makers' risk focus areas, but it overlooks the extreme risk value of inertia reserves. This paper, aimed at inertia reserve planning, can continuously depict the decision-makers' preferences for risk ranges and effectively measure the extreme risk value of inertia reserves, thereby enabling the formulation of differentiated planning schemes. The comparative analysis of this work with existing research is shown in Table 1.

Based on this, this paper proposes a method for power system inertia reserve capacity planning that considers decision-makers' risk preference. The main contributions include: 1) Based on the inertia and primary frequency response characteristics, the system frequency response model with multiple types of source-storage-load regulation resources is established to track the system frequency trajectory after disturbance. 2) Based on the Sequential Monte Carlo method, the system load shedding sets are obtained through probabilistic production simulation. The minimum inertia demand is determined based on RoCoF constraints, and then an inertia mismatch penalty model is constructed to measure the loss caused by RoCoF exceeding limits. 3) The total cost-benefit model of inertia reserve considering risk preferences is established to obtain differentiated planning programs under different accident ranges, and the feasibility of the planning programs is examined to verify the validity of the proposed method based on the improved IEEE-RTS79 system.

II. OBTAINING LOAD SHEDDING SET

To analyze the rationality and feasibility of inertia reserve capacity planning results, it is necessary to simulate the state of system components. Due to the significant uncertainty and temporal fluctuations in the output of wind turbines (WT) and photovoltaic (PV) units, the Markov chain Monte Carlo method is used for probabilistic production simulation [26], [27], as illustrated in Fig. 1.

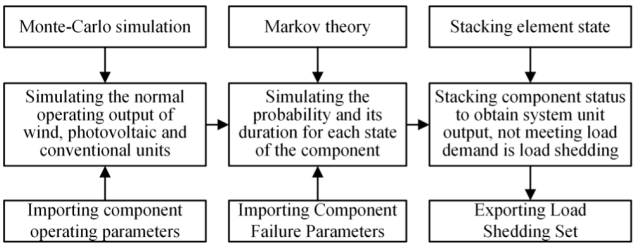

FIGURE 1. Probabilistic product simulation.

A. WIND TURBINE OUTPUT MODEL

1) WIND TURBINE STATE MODEL

During actual operation, due to external environmental factors such as wind speed fluctuations, when the overload causes the unit gearbox oil temperature to reach a critical value and alarm, the wind turbine will enter the derated operation state, and return to normal operation after the alarm is cleared [28]. Therefore, the wind turbine adopts the three-state model as shown in Fig. 2.

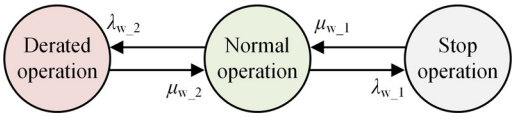

FIGURE 2. Three-state model.

In Fig. 2, λ_{w_1}, λ_{w_2} are the transfer rates of the wind turbine from the operating state to the shutdown and derating state, respectively; μ_{w_1}, μ_{w_2} are the corresponding repair rates.

According to the wind turbine three-state model, the state transfer matrix can be established:

$$T = \begin{bmatrix} 1-(\lambda_{w\_2}+\lambda_{w\_1}) & \lambda_{w\_2} & \lambda_{w\_1} \\ \mu_{w\_2} & 1-\mu_{w\_2} & 0 \\ \mu_{w\_1} & 0 & 1-\mu_{w\_1} \end{bmatrix} \tag{1}$$

By using the Markov method for probabilistic analysis, the duration of each state can be obtained:

$$\begin{cases} \tau_{12} = -\dfrac{1}{\lambda_{w\_2}} \ln u & \tau_{21} = -\dfrac{1}{\mu_{w\_2}} \ln u \\ \tau_{13} = -\dfrac{1}{\lambda_{w\_1}} \ln u & \tau_{31} = -\dfrac{1}{\mu_{w\_1}} \ln u \end{cases} \tag{2}$$

where τ_{12} and τ_{13} are the healthy running time before transitioning to derated and shutdown state in the three-state model, respectively; τ_{21} and τ_{31} are the derated and shutdown time before restoring the healthy running time, respectively. u is a random number uniformly distributed in the interval [0, 1].

2) WIND TURBINE POWER OUTPUT

The power output of wind turbine shows a nonlinear relationship with wind speed, and its power output model can be described by a segmented function [29]:

$$P_w = \begin{cases} 0 & 0 \le v_t \le v_{ci} \\ \left(a + bv_t + cv_t^2\right) P_{wn} & v_{ci} \le v_t \le v_n \\ P_{wn} & v_n \le v_t \le v_{co} \\ 0 & v_t \ge v_{co} \end{cases} \tag{3}$$

where, v_t is the predicted wind speed; v_{ci}, v_n, and v_{co} are the cut-in wind speed, rated wind speed and cut-out wind speed of wind turbine, respectively; P_{wn} is the rated power of the wind turbine; a, b, c are the coefficients to be determined for the power characteristic curve of the wind turbine, which can be solved as follows:

$$\begin{cases} a = \dfrac{1}{(v_{ci}-v_r)^2}\left[v_{ci}^2 + v_{ci}v_r - 4v_{ci}v_r\left(\dfrac{v_{ci}+v_r}{2v_r}\right)^3\right] \\ b = \dfrac{1}{(v_{ci}-v_r)^2}\left[4(v_{ci}+v_r)\left(\dfrac{v_{ci}+v_r}{2v_r}\right)^3 - (3v_{ci}+v_r)\right] \\ c = \dfrac{1}{(v_{ci}-v_r)^2}\left[2 - 4\left(\dfrac{v_{ci}+v_r}{2v_r}\right)^3\right] \end{cases} \tag{4}$$

The wind speed can be obtained by using Weibull distribution method, time series method or machine learning method. For ease of implementation, this paper uses an autoregressive sliding model for wind speed prediction based on historical data.

B. PHOTOVOLTAIC UNIT OUTPUT MODEL

1) PHOTOVOLTAIC UNIT STATE MODEL

Based on the operating characteristics of the photovoltaic unit, its outage model adopts the conventional two-state model shown in Fig. 3.

FIGURE 3. Two-state model.

In Fig. 3, λ_3 and μ_3 are the transfer rate from normal to fault and the fault repair rate of the components in the two-state model, respectively.

The probability and duration of each state of the element can be obtained by probabilistic solution using Markov method:

$$\begin{cases} P_3 = \frac{\mu_3}{\lambda_3+\mu_3} & \tau_3 = -\frac{1}{\lambda_3}\ln u \\ P_4 = \frac{\lambda_3}{\lambda_3+\mu_3} & \tau_4 = -\frac{1}{\mu_3}\ln u \end{cases} \tag{5}$$

where P_3, P_4 are the probabilities that the components are in operation and shutdown, respectively; τ_3, τ_4 are the continuous normal operation time and repair time of the two-state model, respectively.

2) PHOTOVOLTAIC UNIT POWER OUTPUT

The power output of photovoltaic unit has certain volatility and randomness due to external influences such as illumination. Before sunrise, its power output is 0. After sunrise, it gradually increases with the increase of photovoltaic illumination until it reaches the upper limit of power output. Thereafter, it decreases with the light intensity until the power output becomes 0 at sunset; therefore, its power output characteristics can also be described by the segmented function:

$$P_{\text{pv}} = \begin{cases} P_{\text{pvn}} G_{bt}^2 \Big/ (G_{std} R_c) & 0 \le G_{bt} \le R_c \\ P_{\text{pvn}} G_{bt} \Big/ G_{std} & R_c \le G_{bt} \le G_{std} \\ P_{\text{pvn}} & G_{std} \le G_{bt} \end{cases} \tag{6}$$

where G_{std} and P_{pvn} represent the rated solar irradiance and rated power of the photovoltaic unit, respectively. R_{c} is a specific solar irradiance value. G_{bt} is the real-time solar irradiance sequence, which can be obtained from actual measured data or generated by simulation via Homer software.

C. CONVENTIONAL UNIT OUTPUT MODEL

In this paper, conventional units are mainly considered as Thermal Power Unit (TPU), Hydro Power Unit (HPU) and Gas Turbine Unit (GTU). which can be categorized into two states of operation and shutdown according to the actual power system operation process. Therefore, the two-state model shown in Fig. 3 is also adopted for conventional units.

The probability of each state and its duration of the conventional unit is consistent with the calculation method of the photovoltaic unit. when the Monte Carlo random sampling result is less than P_4, the system enters the shutdown state, otherwise it is in the normal operation state. The total power output of conventional units can be obtained based on the capacity and component states of each conventional unit.

D. ACQUISITION OF THE LOAD SHEDDING SET

1) SCREENING OF CONTINUOUS FAULT

The input of inertia reserve is concerned with frequency changes on the second timescale after disturbance, e.g., the difference in the maximum RoCoF before and after the reserve engagement, whereas the sampling timescale for probabilistic production simulation is usually on the hourly scale. When sampling component states, a continuous fault of the same component for l hours obviously has different effects on the system frequency than having l separate faults lasting one hour in different time periods. As shown in Fig. 4, the inertia reserve has already been put into operation at the moment t when the disturbance occurs, and the same disturbance will not trigger the action to maintain system frequency stability multiple times consecutively. By screening the continuous fault states of the units, it is possible to obtain an adapted fault set, where the sampling points $t+1$ to $t+l$ will not affect the system frequency stability and should be filtered out.

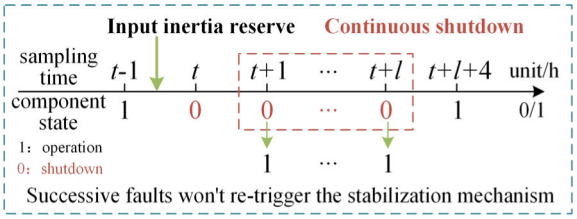

FIGURE 4. Schematic diagram of load shedding.

2) STACKING OF COMPONENT FAULTS

Input the parameters of each component, fault probability, fault repair time, etc., to establish the system component state model. After screening the continuous faults of the component, export the power output of wind power, photovoltaic and conventional units. As shown in Fig. 5, the power output of system units is summed up, and the portion that does not meet the load demand is the disturbance magnitude. Specifically,

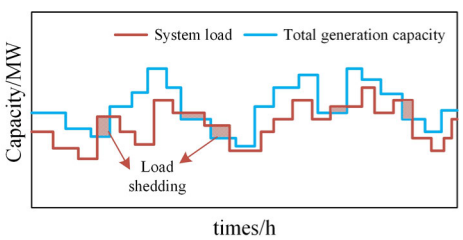

FIGURE 5. Principle of continuous fault screening.

the disturbance magnitude is the ensemble of power shortages due to abnormal operating states of all components under that sampling point.

III. FREQUENCY RESPONSE MODELING

To calculate the difference in system frequency indexes before and after the addition of inertia reserve and to evaluate the benefits generated by the addition of inertia reserve, it is necessary to establish the system frequency response model to accurately track the trajectory of frequency dynamics after system disturbance. Firstly, the frequency response characteristics of conventional units, IBRs and load-side resources are analyzed and modeled, and then a system frequency response model with multiple types of source-storage-load regulation resources is established.

A. CONVENTIONAL UNITS

Conventional units, by virtue of having a physically rotating rotor, can respond spontaneously and without delay when the system is disturbed, which converts rotor kinetic energy into mechanical energy to provide inertia power support. For a synchronous generator, if damping is neglected, the rotor equation of motion can be expressed as:

$$2h_g \frac{df_g}{dt} = \Delta P_{\mathrm{d}} \tag{7}$$

where f_g is the frequency of the generator set, ΔP_e is the disturbed power. h_g is the inertia constant of the generator set, with the unit being seconds. Its physical significance is the time that the generator set at rated speed can last when it utilizes only the kinetic energy stored in the rotor to provide energy for a load of the size of the generator's rated capacity.

Therefore, in the energy perspective, the inertia can also be expressed as:

$$h_g = \frac{E_k}{S_N} = \frac{J\omega^2}{2S_N} \tag{8}$$

where J is the rotational inertia; ω is the mechanical angular velocity; S_N is the rated capacity of the generator set; and E_k is the kinetic energy stored in the rotor, i.e., the quantized value of inertia in the form of energy in MWs.

The primary frequency response characteristics of the three types of conventional units are shown in Fig. 6, and the meanings and value ranges of the relevant parameters in Fig. 6 can be referred to the [30].

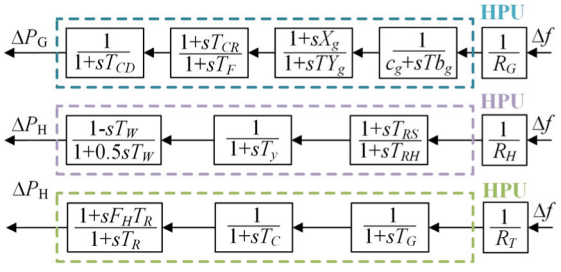

FIGURE 6. Primary frequency regulation characteristics.

B. INVERTER BASED RESOURCES

With the development of virtual inertia technology, IBRs such as wind power, photovoltaic and energy storage (ES) can also provide primary frequency regulation and inertia support capability for the power system. According to the different grid-connection methods and control strategies, IBRs are categorized into grid-following devices and grid-forming devices, both of which have different virtual inertia response characteristics and methods.

In the case of grid-forming devices, the virtual synchronous machine technology not only simulates the external characteristics of the synchronous machine, but also actively establishes the frequency, so it can be regarded as a synchronous generator set.

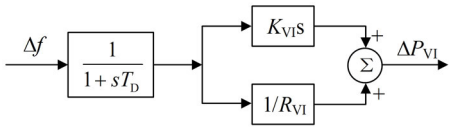

FIGURE 7. Frequency response model of IBR.

At present, most IBRs are grid-following devices, which passively track the grid frequency signal, provide inertia power support in a form like the synchronous inertia response, and participate in primary frequency regulation through virtual droop control. In actual operation, due to the existence of delays in frequency measurement, command generation and control realization, there are delays on the scale of hundred milliseconds for the grid-following IBR to participate in frequency regulation [31]. The generalized model of the frequency response of the IBR is given in Fig. 7, and its transfer function can be expressed as:

$$G_{\mathrm{IBR}} = \frac{\Delta P_{\mathrm{VI}}}{\Delta f} = \frac{K_{\mathrm{VI}} s}{1 + T_{\mathrm{D}}} + \frac{1}{(1 + T_{\mathrm{D}})\, R_{\mathrm{VI}}} \tag{9}$$

where K_{VI} is the virtual inertia coefficient; R_{VI} represents the virtual droop coefficient; and T_D is the response delay time.

Since virtual inertia control has a response delay and cannot respond spontaneously at the instant of system disturbance, it is unable to reduce the maximum RoCoF like synchronous inertia. However, in real grids, any system that relies on the measured frequency and RoCoF will most likely not be able to detect RoCoF up to the theoretical maximum due to the filtering that is unavoidably involved in the frequency measurements [32]. Even if the initial RoCoF exceeds the threshold, the RoCoF relay with a measurement window of hundreds of milliseconds may not be triggered. Therefore, virtual inertia control with a delay of around a hundred milliseconds can still provide effective inertia support.

C. LOAD-SIDE RESOURCE

1) ROTATIONAL INERTIA OF INDUCTION MACHINE

The rotor of Induction Machine (IM) is also electromechanically coupled to the grid and can spontaneously respond to system disturbances, releasing the kinetic energy stored

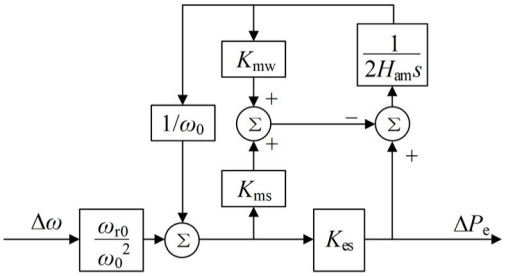

FIGURE 8. Frequency response model of IM.

on the rotor and providing inertia support. As the load-side inertia percentage is increasing, the rotating inertia of the induction machine cannot be neglected.

The frequency response model of the IM is given in Fig. 8 [12]. The frequency response transfer function of induction machine can be expressed as:

$$G_{\mathrm{M}}(S) = \frac{\Delta P_{\mathrm{m}}}{\Delta\omega} = \frac{K_1 s + K_2}{2H_{am}s + K_3} \tag{10}$$

where H_{am} is the inertia time constant of the induction machine, and the meanings of K_1, K_2 and K_3 as well as the related parameters in Fig. 8 are given in the [12].

2) EMERGENCY INTERRUPTIBLE LOAD

For Emergency Interruptible Load (EIL), it is generally connected to the system for control through an internal feeder branch with a low-frequency relay [33], which actively cuts a certain amount of load to make up for the system power deficit when the frequency drops, thus maintaining the system frequency stability. The response characteristics of active load shedding mainly depend on the load shedding control strategy developed or auxiliary service agreement signed between the grid and the EIL provider. Generally, the delayed load-shedding control can be triggered or directly set by the frequency deviation signal.

D. FREQUENCY RESPONSE MODEL CONSTRUCTION

Based on the analysis and modeling of the inertia response and primary frequency regulation characteristics of various types of regulation resources, the frequency response model of the system containing multiple types of regulation resources is established as shown in Fig. 9.

where ΔP_{d} is the power deficit due to system disturbance; H_{sys} and D_{sys} are the system inertia time constant and damping coefficients, respectively; and K_{G}, K_{H}, K_{T}, K_{M}, and K_{I} are the capacity share coefficients of GTU, HPU, TPU, IM, and IBR, respectively.

IV. INERTIA RESERVE CAPACITY PLANNING

The reserve that can significantly improve the system inertia level and effectively reduce the maximum RoCoF is defined as the inertia reserve. Based on the constructed system frequency response model, the frequency dynamic constraints are analyzed. The minimum demand inertia is evaluated

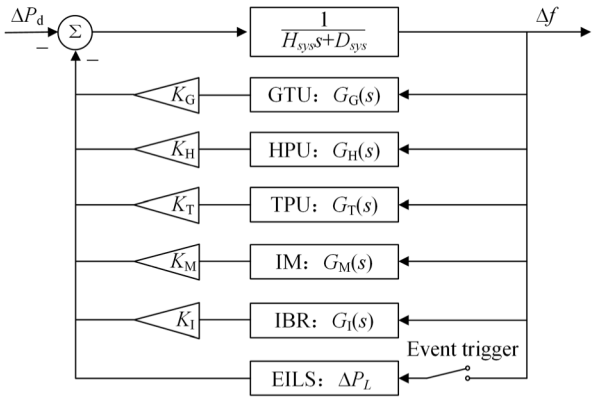

FIGURE 9. System frequency response model.

considering RoCoF constraints to characterize the risk of inertia exceeding limits. The consequence of RoCoF exceeding limits is analyzed to construct a penalty model to measure the loss of exceeding limits. The reserve cost-benefit analysis is performed based on risk preferences, and the feasibility of the planning results is verified.

A. EVALUATION OF MINIMUM DEMAND INERTIA

1) FREQUENCY DYNAMIC CONSTRAINT ANALYSIS

The existing minimum demand inertia evaluation is mainly based on the frequency nadir constraints and RoCoF constraints to find the minimum inertia required by the system to guarantee the grid frequency stability under the expected faults [34]. However, unlike the theoretical evaluation, the minimum demand inertia evaluation for inertia reserve planning should focus on the RoCoF constraints, considering the specific needs and response characteristics of inertia reserve. In other words, the RoCoF constraints should be prioritized over the frequency nadir constraints in the inertia reserve planning process.

In the time scale, the inertia acts at the initial period of frequency response containing the disturbance instant, Insufficient inertia will directly lead to the ROCOF exceeding limits, and the subsequent means can no longer undo the fact that the maximum ROCOF exceeds limits. While for the frequency nadir constraint, if the inertia and primary frequency regulation capability are insufficient, it can also be curbed by Under Frequency Load Shedding (UFLS) and other measures.

In terms of economic metrics, inertia resources generally have much higher investment and utilization costs than primary frequency regulation resources due to the extremely high response speed requirements. When the system inertia already meets the RoCoF constraint but not the frequency nadir constraint, the frequency nadir can be intercepted by means of calling fast frequency response resources. If the grid inertia is raised to curb the maximum frequency deviation, not only the effect is poor, but also far less cost-effective

than investing in primary frequency regulation to intercept the frequency nadir.

2) MINIMUM DEMAND INERTIA ASSESSMENT

Numerous national grids currently set clear limits on RoCoF. In the UK, the RoCoF protection is set to 0.125 Hz/s, which is exceeded to cause distributed generation to go off-grid [5]. Newly installed generator protection devices in countries such as the United States limit RoCoF to 0.5 Hz/s. Power system stabilization guidelines require that RoCoF cannot exceed 2 Hz/s within 0.5 seconds after the disturbance occurs, 1.5 Hz/s within 1 second, and 1.25 Hz/s within 2 seconds [35]. At present, the relevant standards for Chinese power grids do not provide clear constraints on system-level and equipment-level RoCoF protection.

Based on (7), the minimum inertia required for the system to satisfy the RoCoF constraints under the expected disturbance ΔP_{d} can be expressed as:

$$H_{\min} = \frac{\Delta P_d}{2RoCoF_{\max}} \tag{11}$$

From (11), the larger the disturbance or the stricter the RoCoF constraint, the larger the minimum inertia required by the system. Inputting the systems load shedding set obtained from the probabilistic production simulation into (11), the minimum inertia demand of the system under different RoCoF constraints can be obtained and compared with the actual inertia, which can portray the risk of inertia exceeding limits. Different RoCoF constraint levels can reflect the grid decision-makers' concern about the risk range and the degree of inertia demand.

B. PENALTY MODEL FOR ROCOF EXCEEDING LIMITS

The system inertia is directly linked to the RoCoF indicator. As the inertia level continues to decrease, the RoCoF will continue to rise after the grid is disturbed. Once the RoCoF exceeds limits, it may cause damage to synchronous units, distributed generation going off-grid and further deterioration of the frequency drop, which will cause losses that cannot be accurately measured.

When planning for inertia reserve, it is necessary to constrain the RoCoF and measure the loss caused by RoCoF exceeding limits, thus providing a guiding basis for decision-makers to plan for inertia reserve capacity. When the loss caused by RoCoF exceeding limits is less than the cost of equipping inertia resources, grid decision-makers may tend to set less inertia reserve. When the RoCoF exceeds limits due to insufficient inertia reserve capacity, resulting in system loss far exceeding the cost of additional reserve, grid decision-makers will tend to set more inertia reserve capacity. Therefore, measuring the system loss caused by RoCoF exceeding limits is critical to the decision-making scheme.

The consequences of RoCoF exceeding limits are sorted out and analyzed, and there are three categories of losses caused by it. Firstly, excessive RoCoF may cause the synchronous unit having the slip pole phenomenon, resulting in internal structural damage. The synchronous unit needs to be repaired and replaced. Secondly, excessive RoCoF may trigger the relay protection setting value of distributed generation, resulting in the distributed generation going off-grid, further increasing the system power deficit, and making the frequency drop even worse. Distributed generation off-grid will cause economic losses, frequency deterioration will also make the UFLS losses increase. In addition, excessive RoCoF may cause the system frequency to collapse before the governor and other frequency regulation means have time to act, at which point the damage to the system will be difficult to measure. This situation belongs to the high-loss low-probability events, generally occurring in extreme accident scenarios.

Based on the above analysis, the losses caused by RoCoF exceeding limits mainly include synchronous unit damage, distributed generation off-grid losses, UFLS losses due to frequency deterioration, and system frequency collapse losses in extreme scenarios. At the equipment level, different units have different RoCoF tolerance capabilities, and the protection setting values of different distributed generation are also different, e.g., wind turbines can continue to operate stably with RoCoF as high as 4 Hz/s, while synchronous units are recommended not to exceed 2 Hz/s [35]. At the system level, the amount and capacity of distributed generation within different regions and grids, the losses of UFLS after frequency deterioration are also different. In addition, if considering the frequency spatial and temporal distribution characteristics [36], the frequency dynamics in different regions and grids are not the same, and the situations of RoCoF exceeding limits are also not the same. Therefore, to measure the loss caused by RoCoF exceeding limits, it is necessary to vary from network to network and from region to region.

Currently, there are fewer studies on the loss caused by RoCoF exceeding limits. Based on the relevant RoCoF constraints at home and abroad, and combined with the above loss analysis, the penalty model for RoCoF exceeding limits can be constructed as follows:

$$C_{RoCoF} = \begin{cases} 0 & 0 \le RoCoF < R_1 \\ C_1 & R_1 \le RoCoF < R_2 \\ \vdots & \vdots \\ C_{m-1} & R_{m-1} \le RoCoF < R_m \\ C_m & RoCoF \ge R_m \end{cases} \tag{12}$$

where R_1, R_2, R_{m-1} and R_m are different levels of RoCoF constraints, which depend on the relay protection setting value of distributed generation and the RoCoF tolerance value of units within the grid; C_1, C_2, C_{m-1} and C_m are the loss values corresponding to RoCoF out of limits, which depend on factors such as off-grid situation of distributed generation, damage of synchronized units and incremental cost of UFLS under the corresponding RoCoF constraints.

The higher the RoCoF, the more severe the loss, so C_1, C_2, C_{m-1} and C_m show an increasing law. From the reserve

planning level, the severity of RoCoF cross-limit will affect the decision-maker's planning scheme. The more severe the RoCoF cross-limit loss is, the stronger the decision maker's determination to plan the inertia reserve capacity will be, and the more adequate capacity will be planned in the end. Therefore, the results of inertia reserve planning will be different for different power grids in different regions, which should be adapted to the local conditions.

C. ACQUISITION OF RESERVE PLANNING PROGRAMS

1) RISK PREFERENCE COST-BENEFIT ANALYSIS

In the inertia reserve planning problem, the more extreme the events concerned by the decision-maker, the greater the losses caused by RoCoF out of limits, corresponding to a higher risk value. Under inertia reserve capacity r, different incident levels cause different losses, and this type of cost is called reliability cost. The reliability cost L is a random variable and there exists a probability distribution associated with the reserve capacity r. Let the probability density distribution function be $p_L(x, r)$. To consider the decision-maker's risk preference, the risk scope of its concern, i.e., the severity and rarity of the loss that the decision-maker is interested in during the global accident, is reflected by defining the risk factor γ. In this paper, the risk factor is quantified by the probability that the reliability cost L is greater than or equal to some threshold C_L:

$$\gamma = \int_{C_L}^{+\infty} p_L(x, r)\, dx = \varphi_L(C_L, r) \tag{13}$$

$$C_L = \varphi_L^{-1}(\gamma, r) \tag{14}$$

The risk factor γ is the proportion of accidents in the whole accident set that the grid dispatchers are most concerned about. By changing γ, the decision-maker's concern for different risk ranges can be changed, and thus the change of risk preference can be continuously portrayed. When the risk factor γ tends to 0, the decision-maker is more inclined to pay attention to the extreme accidents that threaten the frequency stability. And when the γ tends to 1, the decision-maker is more inclined to pay attention to the global accidents. Therefore, the conditional reliability cost associated with reserve capacity r under risk factor γ can be expressed as:

$$L(\gamma, r) = E(L \,|L \geq C_R) = \frac{\int_{\varphi_L^{-1}(\gamma,r)}^{+\infty} x \cdot p_L(x, r)\, dx}{\gamma} \tag{15}$$

To better demonstrate the validity and feasibility of the proposed method and model, this paper is compared and analyzed with the VaR analysis method in the literature [23]. The essential difference between the VaR method and the proposed method is that the VaR method discards some of the extreme risk events in the risk analysis process, while this paper discards the frequent low-risk events with little threat to frequency security. The planning results of the two methods can be compared and analyzed to demonstrate the superiority of the conditional risk preference analysis method proposed in this paper. Corresponding to the risk factors defined in this paper, the corresponding VaR formula is defined as follows:

$$\begin{cases} V_{aR}(\gamma, r) = \max\left\{V_{VaR} \in \varphi_V^{-1}(\gamma, r)\right\} \\ \int_{T_V}^{+\infty} p_V(x, r)\, dx \leq (1-\gamma) \end{cases} \tag{16}$$

where the value of $V_{aR}(\gamma, r)$ is the worst system loss due to RoCoF overrun when the system is equipped with inertia reserve of capacity r without exceeding the extreme risk factor γ.

Let N RoCoF out of limits incidents occur in the system in the nth year, the losses of RoCoF out of limits in year n with reserve capacity r can be calculated:

$$L_n(r) = \sum_{i=1}^{N} C_{RoCoF,i} \tag{17}$$

In practice, the loss distribution of RoCoF exceeding limits under the global risk range can be calculated based on the system load shedding set from the probabilistic production simulation. The reliability cost is then ranked, and different risk ranges can be selected based on their discrete probability distributions, to find the reliability cost after installing inertia reserve r under different risk factors γ.

By increasing the inertia reserve, the RoCoF can be effectively slowed down, thus reducing the RoCoF cross-limit loss and improving the reliability of the system. The reduction of RoCoF cross-limit loss before and after adding inertia reserve is the reliability gain. Therefore, the reliability gain of inertia reserve considering risk preference can be expressed as:

$$E(\gamma, r) = L(\gamma, r) - L(\gamma, 0) \tag{18}$$

2) THE TOTAL COST-BENEFIT MODEL OF RESERVE

The cost of adding inertia reserve mainly includes the investment cost $I(r)$ and utilization cost $D(r)$. Retrofitting retired thermal power units into synchronous regulators, building flywheel energy storage, or installing power electronics to provide virtual inertia can all provide means of supporting inertia reserve. In reserve planning, the equal annual value method is often used to calculate the investment cost for the sample year. The utilization cost is related to the effective times n of RoCoF exceeding limits, the inertia capacity demand H_r after RoCoF exceeding limits, and the unit inertia utilization cost d.

$$F(r) = I(r) + D(r) \tag{19}$$

$$I(r) = B(r)\, \frac{k(1+k)^{\alpha}}{(1+k)^{\alpha} - 1} \tag{20}$$

$$D(r) = \sum_{i=1}^{n} H_{r,i} \cdot d \tag{21}$$

where k is the discount rate, σ is the life cycle of the inertia reserve resources, and B represents the total investment cost.

By combining the inertia reserve reliability benefits and the cost of additional reserve obtained from (18) and (19), an analytical model of the total cost-benefit analysis of reserve that

considers risk preference can be established:

$$M(\gamma, r) = E(\gamma, r) - F(\gamma, r) \tag{22}$$

Taking the maximization of final income $M(\gamma, r)$ as the objective function, setting the optimization interval of inertia reserve capacity, and obtaining the set of load shedding by probabilistic production simulation in year Y. The optimal inertia reserve capacity under different risk ranges can be obtained by iteratively altering the decision-maker's risk preference through the risk factor γ.

3) PROGRAM FEASIBILITY VERIFICATION

Decision-makers' risk preference carries subjective judgment of accident severity, and it is necessary to check the feasibility of the planning results and give confidence indicators, which will help the decision maker to avoid the reserve planning not meeting the actual demand due to subjective experience.

In the inertia reserve planning process, the total cost $A(r)$ includes the cost of additional inertia reserve and the reliability cost of RoCoF exceeding limits, which also exists a probability distribution associated with the reserve capacity r. Then, analogously to (15), the total cost under the risk factor γ can be expressed as follows:

$$A(\gamma, r) = E(A \,|A \geq C_A) = \frac{\int_{C_A}^{+\infty} x \cdot p_A(x, r)\, dx}{\gamma} \tag{23}$$

Then the confidence indicator of the planning program can be defined as:

$$\sigma(\gamma, r) = 1 - \frac{A(\gamma, r)}{A(\gamma, 0)} \tag{24}$$

According to this indicator, it can be judged whether the additional inertia reserve r is too costly to be adopted under the risk factor γ. When σ is less than 0, the planning scheme should be rejected; when σ is greater than or equal to 0, the planning scheme can be adopted, and the larger the confidence indicator is, the more worthy the scheme is to be adopted.

V. CASE STUDIES

To validate the feasibility and effectiveness of the proposed planning scheme, the improved IEEE RTS-79 test system is used for case studies. The effect of input inertia reserve is analyzed, and the risk factor is changed to analyze the impact of decision maker's risk preference on the planning scheme. The RoCoF differential cross-limit loss is set to analyze the variability of the planning scheme in different grids and regions. And finally, the feasibility of the planning scheme is validated and analyzed.

A. INTRODUCTION TO THE TEST SYSTEM

Considering the large-scale integration of new energy units into the power grid, the nuclear power units in the IEEE RTS-79 system are replaced by wind turbines and photovoltaic units, and the system structure is shown in Fig. 10. The installed capacity of each unit in the improved system and its

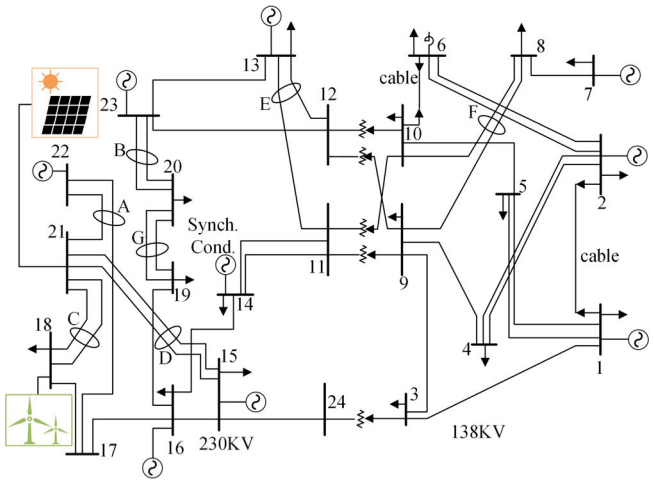

FIGURE 10. IEEE RTS-79 test system.

percentage are shown in Table 2. The virtual droop coefficient R_v is set at 0.05, and the control delay is 0.1s.

TABLE 2. System units parameters.

Unit type	Inertia constant/s	Capacity/MW	Percentage/%
TPU	7.25	2225	58.17
HPU	4.820	300	7.84
GTU	9	80	2.09
WT	/	900	23.54
PV	/	300	7.84
ES	/	20	0.52
Total	4.784	3825	100

The fault parameters of the relevant components in the probabilistic production simulation are shown in the [25]. The inertia reserve resource takes synchronous regulator as an example, and its investment cost is $37,727.3/MWs. Considering the synchronous unit provides the inertia support at no cost, and the utilization cost is set to 0. The reserve life cycle is set to 30a, and the discount rate is taken to be 10%. The loss of RoCoF exceeding limits is set as shown in Table 3, and L_b is taken to be 18, which can be flexibly corrected in accordance with the practical situation of the different regional power grids.

B. INERTIAL RESERVE CAPACITY PLANNING

1) ANALYSIS OF THE EFFECT OF RESERVE INPUT

Based on the constructed frequency response model, the system frequency dynamic trajectory is tracked before and after the addition of inertia reserve to measure the effect of reserve input. When a 750MW disturbance (0.2 of the system generating capacity) occurs in the system, the trajectories of system frequency change after adding different sizes of inertia reserve are shown in Fig. 11. After adding inertia

TABLE 3. Loss of RoCoF exceeding limits.

Lost rounds	RoCoF threshold /(Hz/s)	Loss/10^3\$
1	0.125	1*L_b
2	0.5	4* L_b
3	0.75	5* L_b
4	1.0	9* L_b
5	1.25	10* L_b
6	1.5	16* L_b
7	1.75	17* L_b
8	2.0	30* L_b

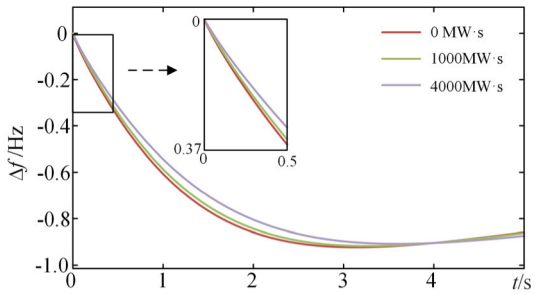

FIGURE 11. System frequency response curves for different reserve capacities.

reserve, the system RoCoF is significantly slowed down, and the larger the inertia reserve capacity is, the more obvious the effect is.

Further, based on the load shedding set from probabilistic production simulation, the economic benefit of additional reserve is measured by obtaining the inertia reserve capacity planning scheme based on the global average risk when the risk factor γ is taken to be 1. Fig. 12 shows the process of finding the optimal inertia reserve capacity under the global risk range.

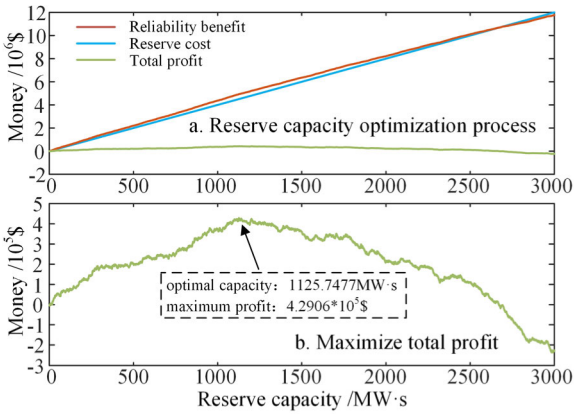

FIGURE 12. Reserve capacity optimization process under global risk range.

With the increase of additional inertia reserve capacity, the reliability benefit and reserve cost both increase, and the two growth rate is consistent when the reserve capacity $r = 1125.7477$MWs. According to the law of marginal cost-benefit analysis, the total benefit reaches the maximum of $4.2906*10^5$\$, so it is the optimal inertia reserve planning scheme under the average risk level. By adding inertia reserve, RoCoF can be effectively reduced to improve system reliability. However, the analysis based on average risk will result in small-probability high-loss events being submerged in many common small-loss events, and the decision-maker will unable to perceive the specific risk range and carry out targeted planning schemes.

2) ANALYSIS OF RISK PREFERENCE OF DECISION MAKERS

By the iterative risk factors to find the optimal inertia reserve capacity under different risk ranges, the influence of decision-maker's risk preference on the reserve planning scheme can be effectively portrayed. Table 4 gives the optimal inertia reserve capacity and the related cost-benefit amount under different risk factors. Fig. 13 and Fig. 14 show some of the reserve optimization results under the high-risk factor and low risk factor, respectively.

TABLE 4. Optimal capacity and its cost-benefit under partial γ.

γ	Optimal capacity/MW • s	Total profit/\$	Reliability benefit /\$	Reserve cost/\$
0.01	30505.79	1.54×10^8	2.76×10^8	1.22×10^8
0.03	26166.53	1.19×10^8	2.24×10^8	1.05×10^8
0.05	22575.96	8.86×10^7	1.79×10^8	9.04×10^7
0.10	17601.31	6.76×10^7	1.38×10^8	7.04×10^7
0.30	9572.91	3.83×10^7	7.66×10^7	3.83×10^7
0.60	3963.34	6.00×10^6	2.19×10^7	1.59×10^7
0.80	3040.80	2.70×10^6	1.49×10^7	1.22×10^7
1.00	1125.75	4.30×10^5	4.94×10^6	4.51×10^6

The risk factor γ is smaller, the more the decision-maker prefers to focus on small-probability high-loss events in global accidents, the higher the additional inertia reserve capacity is required, and the more the total profit of additional inertia reserve is considerable. If the reserve capacity planning is based on the average risk, it will reduce the sensitivity of the decision-maker to the high-risk range, which will also affect the decision-maker's determination to increase the inertia reserve, and will lead to the decision-maker underestimating the inertia reserve demand in high-risk incidents.

From Table 4, Fig. 13, and Fig. 14, it is easy to find that the decision-maker's risk preference has a critical impact on the planning results of inertia reserve capacity. As the risk factor decreases, the risk range of the decision-maker's concern is from average to extreme, and the optimal inertia reserve capacity increases from 1125.75 MWs to 30505.79 MWs, which indicates that the necessity and determination of

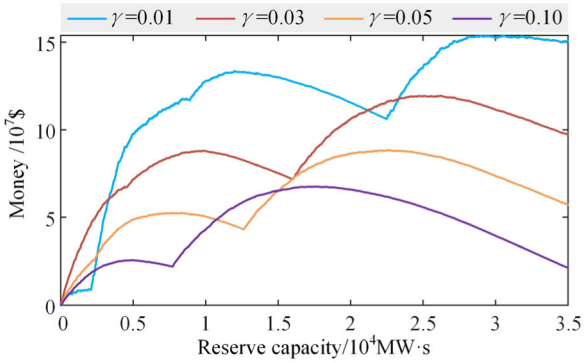

FIGURE 13. Partial reserve capacity optimization process under higher risk ranges.

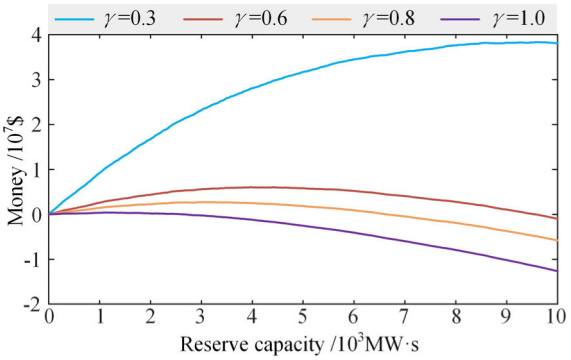

FIGURE 14. Partial reserve capacity optimization process under lower risk ranges.

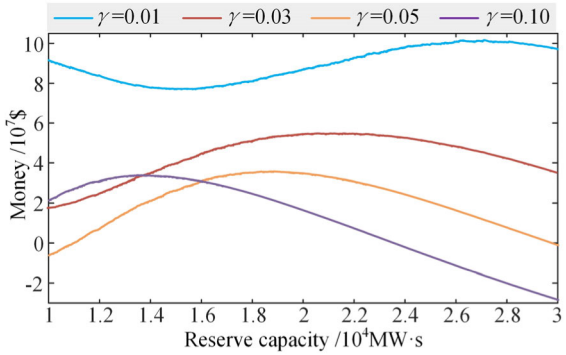

FIGURE 15. Partial reserve capacity optimization process at higher risk ranges under the VaR method.

TABLE 5. Optimization result comparison.

γ	Optimal capacity by VaR/MW • s	Total profit by VaR/$	Optimal capacity by cVaR /MW • s	Total profit by cVaR /$
0.01	27108.33	1.02×10^{8}	30505.79	1.54×10^{8}
0.03	20624.89	5.51×10^{7}	26166.53	1.19×10^{8}
0.05	18842.96	3.60×10^{7}	22575.96	8.86×10^{7}
0.10	13482.13	3.53×10^{7}	17601.31	6.76×10^{7}
0.3	3739.41	3.14×10^{7}	9572.91	3.83×10^{7}
0.35	2427.99	1.13×10^{7}	8537.52	2.78×10^{7}
0.4	427.43	4.93×10^{5}	7861.69	2.03×10^{7}

adding inertia reserve increase as the accident loss the decision maker's concern tends to be extreme. On the other hand, as the risk factor decreases, both the reliability benefit and the total profit from adding inertia reserve increase significantly. The more severe the accident losses, the more significant the benefits of adding inertial reserve, and the more necessary inertia reserve becomes.

In the actual grid inertia reserve planning, decision-makers can focus on specific risk ranges based on operational experience and the risk tolerance of grids, and develop planning schemes for inertia reserve capacity under different risk preferences for selection.

3) COMPARISON WITH VAR METHOD

To better demonstrate the validity and feasibility of the reserve planning method proposed in this paper, the more widely used VaR analysis method is used as a comparative case. The optimal inertia reserve capacity based on the VaR method and the related cost-benefit amount under some risk factors are given in Table 5 and compared with the optimization results of the method proposed in this paper. The optimal reserve capacity optimization process for some high risk ranges is given in Fig. 15.

As can be seen from Table 5 and Fig. 15, the benefits obtained from the VaR approach are lower than those from cVaR approach proposed in this paper under different risk factors. Although the adoption of the VaR method can consider the decision maker's risk preference, it still discards some of the extreme events in the risk range of concern. While the inertia reserve is specifically set up for high-risk events that threaten the frequency stability of the system, therefore the planning program needs to be more sensitive and targeted to the risk of system frequency instability. It is obvious that the method proposed in this paper can better characterize the risk value of extreme events and develop more targeted planning schemes than the traditional VaR method.

4) ANALYSIS OF LOSS FROM ROCOF EXCEEDING LIMITS

The decision-maker's concern and preference for the risk range generally depends on its assessment of the accident level it can tolerate and its ability to withstand losses. Capacity planning for inertia reserve needs to measure the losses caused by RoCoF exceeding limits to assess the risk range that can be tolerated. The losses caused by RoCoF exceeding limits need to vary from network to network and from place to place. The more serious the losses caused by RoCoF exceeding limits, the stronger the decision-maker's determination to plan for inertia reserve capacity will be, and the more adequate the planned capacity will be in the end. Therefore, the results of inertia reserve planning will be different for different grids in different regions.

TABLE 6. Optimal reserve capacity under different loss of RoCoF exceeding limits.

γ	Optimal capacity/MW • s				
	L_b=16	L_b=17	L_b=18	L_b=19	L_b=20
0.01	28976.43	28978.35	30505.79	30505.79	31798.31
0.03	24132.96	24673.70	26166.53	26166.53	26265.31
0.05	21637.61	22575.96	22575.96	22594.95	23490.4
0.10	16556.06	17110.29	17601.31	18336.45	18336.45
0.30	8537.51	8587.45	9572.91	10625.11	10625.11
0.60	3484.72	3963.31	3963.34	4626.49	4626.49
0.80	2440.4	2527.7	3040.8	3484.72	3963.33
1.00	282.92	1125.75	1125.75	1761.75	2440.39

TABLE 7. Total profit capacity under different loss of RoCoF exceeding limits.

γ	Total profit/$				
	L_b=16	L_b=17	L_b=18	L_b=19	L_b=20
0.01	1.24×10^8	1.39×10^8	1.54×10^8	1.69×10^8	1.85×10^8
0.03	9.51×10^7	1.07×10^8	1.19×10^8	1.32×10^8	1.44×10^8
0.05	6.86×10^7	7.85×10^7	8.86×10^7	9.84×10^7	1.08×10^8
0.10	5.25×10^7	6.00×10^7	6.76×10^7	7.52×10^7	8.30×10^7
0.30	3.01×10^7	3.42×10^7	3.83×10^7	4.26×10^7	4.71×10^7
0.60	3.73×10^6	4.85×10^6	6.00×10^6	7.37×10^6	8.73×10^6
0.80	1.25×10^6	1.95×10^6	2.70×10^6	3.64×10^6	4.61×10^6
1.00	4.32×10^4	1.55×10^5	4.30×10^5	7.60×10^5	1.25×10^6

The optimal inertia reserve capacity corresponding to each risk factor under different RoCoF cross-limit loss and its total profit are given in Tables 6 and 7, respectively. It is easy to see that with the increase of loss due to RoCoF exceeding limits, the optimal inertia reserve capacity under different risk ranges is increasing, and the total profit generated by additional inertia reserve is also rising. In other words, the weaker the grid's ability to withstand RoCoF exceeding limits, the higher the demand for additional inertia reserve, and the more considerable the benefit of additional inertial reserve. On the contrary, if the grid's inertia is sufficient, and the components are more tolerant to RoCoF exceeding limits, the need for additional inertia reserve will be reduced accordingly. Therefore, different inertia reserve planning schemes should be formulated for different grids in different regions, according the actual situation.

C. PLANNING PROGRAM VERIFICATION

Decision-makers' risk preference are subjective, and the inertia reserve program under different risk factors need to be verified, and the corresponding confidence indicator are given to judge the feasibility of the program. Taking the optimal reserve capacity of 9572.91 MWs when the risk factor is 0.3 as an example for the feasibility check, Fig. 16 gives the confidence indicator of the planning program under different risk factors and the total cost before and after additional reserve.

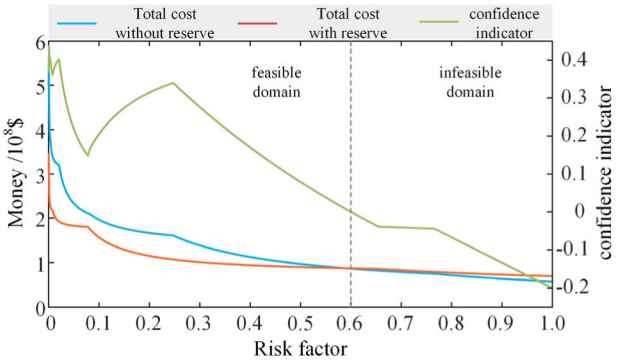

FIGURE 16. Verification of the planning program's feasibility.

When the risk factor is 0.6, the confidence indicator of the program is 0, and the program is at the boundary between feasible and infeasible. When the risk factor is less than 0.6, the reserve capacity is acceptable under different risk ranges, and the smaller the risk factor, the higher the confidence indicator, the higher the feasibility of the planning program. On the contrary, when the risk factor is greater than 0.6, the planning program is in the infeasible domain. In this case, the total cost of adding inertia reserve is too high, and the planning program should be rejected.

VI. CONCLUSION

In this paper, we add inertia reserve and propose an inertia reserve capacity planning method considering the risk preference of decision makers for the problem of increasing inertia scarcity in power systems, to ensure the adequacy of grid inertia from the reserve planning level. The theoretical study and case analysis show that:

- As the system synchronous inertia continues to decrease, the risk of frequency overrun is increasing, and it is necessary to constrain the RoCoF and formulate a reasonable overrun penalty mechanism according to the network and local conditions. The addition of inertia reserve can effectively improve the system inertia level, and then improve the risk response capability of the system for extreme events.
- The proposed inertia reserve planning method is more sensitive to the risk value of extreme events, and can consider the decision-maker's risk preference to formulate planning schemes under different risk ranges, thus avoiding the homogenization of extreme events and improving the system's risk response capability for extreme events. The more severe the accidental losses that the decision maker is concerned about, the larger the additional inertia reserve capacity is required and the more significant the benefits of the additional reserve can be.
- Different grids have different risk tolerance and security level requirements, and different losses caused by

RoCoF exceeding limits. The more serious the consequences of RoCoF exceeding limits, the stronger the decision-maker's determination to set up inertia reserve, and the higher the capacity and benefit of setting up inertia reserve. For different power grids, it is necessary to formulate different inertia reserve planning programs according to the actual situation.

This paper only focuses on inertia reserve capacity planning, failing to realize the optimal coordinated planning between inertia and primary frequency regulation reserve, and failing to realize the optimal allocation of multiple types of inertia resources, which has certain limitations. In the future, we will plan multiple flexibility resources in a coordinated manner to realize the optimal joint planning allocation of inertia and primary frequency regulation reserve which considers the risk preference of decision makers, to guarantee the power system's ability to cope with extreme events.

REFERENCES

[1] P. Hu, Y. Li, Y. Yu, and F. Blaabjerg, "Inertia estimation of renewable-energy-dominated power system," *Renew. Sustain. Energy Rev.*, vol. 183, Sep. 2023, Art. no. 113481.

[2] P. M. Anderson and A. A. Fouad, *Power System Control and Stability*. Hoboken, NJ, USA: Wiley, 2002.

[3] E. Heylen, F. Teng, and G. Strbac, "Challenges and opportunities of inertia estimation and forecasting in low-inertia power systems," *Renew. Sustain. Energy Rev.*, vol. 147, Sep. 2021, Art. no. 111176.

[4] M. Zhang, S. S. Yu, H. Yu, P. Li, W. Li, and S. M. Muyeen, "Dispatchable capacity optimization strategy for battery swapping and charging station aggregators to participate in grid operations," *Energy Rep.*, vol. 10, pp. 734–743, Nov. 2023.

[5] H. Sun, T. Xu, Q. Guo, Y. Li, W. Lin, J. Yi, and W. Li, "Analysis on blackout in great Britain power grid on August 9th, 2019 and its enlightenment to power grid in China," in *Proc. CSEE*, Nov. 2019, vol. 39, no. 21, pp. 6183–6191.

[6] H. Zeng, F. Sun, T. Li, Q. Zhang, J. Tang, and T. Zhang, "Analysis of '9.28' blackout in South Australia and its enlightenment to China," *Autom. Electr. Power Syst.*, vol. 41, no. 13, pp. 1–6, Jul. 2017.

[7] B. Tan and J. Zhao, "Data-driven time-varying inertia estimation of inverter-based resources," *IEEE Trans. Power Syst.*, vol. 38, no. 2, pp. 1795–1798, Mar. 2023.

[8] L. Shang, X. Dong, C. Liu, and Z. Gong, "Fast grid frequency and voltage control of battery energy storage system based on the amplitude-phase-locked-loop," *IEEE Trans. Smart Grid*, vol. 13, no. 2, pp. 941–953, Mar. 2022.

[9] M. Li, W. Huang, N. Tai, L. Yang, D. Duan, and Z. Ma, "A dual-adaptivity inertia control strategy for virtual synchronous generator," *IEEE Trans. Power Syst.*, vol. 35, no. 1, pp. 594–604, Jan. 2020.

[10] J. Boyle, T. Littler, and A. M. Foley, "Coordination of synthetic inertia from wind turbines and battery energy storage systems to mitigate the impact of the synthetic inertia speed-recovery period," *Renew. Energy*, vol. 223, Mar. 2024, Art. no. 120037.

[11] J. Liang, H. Fan, L. Cheng, S. Rong, T. Li, T. Yu, and L. Wang, "Control strategy for improving the frequency response characteristics of photovoltaic and energy storage systems based on VSG control," *Energy Rep.*, vol. 11, pp. 2295–2305, Jun. 2024.

[12] T. Zhou, Z. Chen, Y. Wang, and Z. Liu, "Evaluation of minimum inertia in power systems considering frequency response of induction machines," *Power Syst. Prot. Control*, vol. 50, no. 20, pp. 22–31, Oct. 2022.

[13] L. Chen, X. Wang, Y. Min, G. Li, L. Wang, J. Qi, and F. Xu, "Modelling and investigating the impact of asynchronous inertia of induction motor on power system frequency response," *Int. J. Electr. Power Energy Syst.*, vol. 117, May 2020, Art. no. 105708.

[14] Z. Peng, Q. Peng, Y. Zhang, H. Han, Y. Yin, and T. Liu, "Online inertia allocation for grid-connected renewable energy systems based on generic ASF model under frequency nadir constraint," *IEEE Trans. Power Syst.*, vol. 39, no. 1, pp. 1–13, Jan. 2023.

[15] Y. Shen, W. Wu, B. Wang, and S. Sun, "Optimal allocation of virtual inertia and droop control for renewable energy in stochastic look-ahead power dispatch," *IEEE Trans. Sustain. Energy*, vol. 14, no. 3, pp. 1–12, Jul. 2023.

[16] M. Zhang, W. Li, S. S. Yu, K. Wen, and S. M. Muyeen, "Day-ahead optimization dispatch strategy for large-scale battery energy storage considering multiple regulation and prediction failures," *Energy*, vol. 270, May 2023, Art. no. 126945.

[17] M. Zhang, W. Li, S. S. Yu, H. Wang, and Y. Ba, "Optimal day-ahead large-scale battery dispatch model for multi-regulation participation considering full timescale uncertainties," *Renew. Sustain. Energy Rev.*, vol. 189, Jan. 2024, Art. no. 113963.

[18] Q. Hu, R. Han, X. Quan, Z. Wu, C. Tang, W. Li, and W. Wang, "Grid-forming inverter enabled virtual power plants with inertia support capability," *IEEE Trans. Smart Grid*, vol. 13, no. 5, pp. 4134–4143, Sep. 2022.

[19] A. van Stiphout, K. De Vos, and G. Deconinck, "The impact of operating reserves on investment planning of renewable power systems," *IEEE Trans. Power Syst.*, vol. 32, no. 1, pp. 378–388, Jan. 2017.

[20] Z. Lu, J. Jiang, Y. Qiao, Y. Min, and H. Li, "A review on generalized inertia analysis and optimization of new power systems," *Proc. CSEE*, vol. 43, no. 5, pp. 1754–1776, Mar. 2023.

[21] Z. Liang, R. Mieth, and Y. Dvorkin, "Inertia pricing in stochastic electricity markets," *IEEE Trans. Power Syst.*, vol. 38, no. 3, pp. 2071–2084, May 2023.

[22] L.-R. Chang-Chien, L. N. An, T.-W. Lin, and W.-J. Lee, "Incorporating demand response with spinning reserve to realize an adaptive frequency restoration plan for system contingencies," *IEEE Trans. Smart Grid*, vol. 3, no. 3, pp. 1145–1153, Sep. 2012.

[23] M. Choudhry, *An Introduction to Value-at-Risk*. Hoboken, NJ, USA: Wiley, Jan. 2012.

[24] G. Zhang, W. Wu, and B. Zhang, "Optimization of operation reserve coordination considering wind power integration," *Autom. Electr. Power Syst.*, vol. 53, no. 12, pp. 15–19, Jun. 2011.

[25] Z. Li, W. Li, S. S. Yu, L. Guo, H. Zheng, J. Ma, L. Zhao, W. Dou, and N. Zhang, "Fast frequency response reserve planning for power systems considering homogeneous extreme risks," *IEEE Trans. Ind. Appl.*, vol. 59, no. 2, pp. 2314–2325, Mar. 2023.

[26] B. Tan, J. Zhao, M. Netto, V. Krishnan, V. Terzija, and Y. Zhang, "Power system inertia estimation: Review of methods and the impacts of converter-interfaced generations," *Int. J. Electr. Power Energy Syst.*, vol. 134, Jan. 2022, Art. no. 107362.

[27] M. Zhao, R. Zhang, C. Lin, H. Zhou, and J. Shi, "Stochastic model predictive control for dual-motor battery electric bus based on signed Markov chain Monte Carlo method," *IEEE Access*, vol. 8, pp. 120785–120797, 2020.

[28] P. Guo and D. Infield, "Wind turbine power curve modeling and monitoring with Gaussian process and SPRT," *IEEE Trans. Sustain. Energy*, vol. 11, no. 1, pp. 107–115, Jan. 2020.

[29] F. Ying, Y. Jiang, M. He, H. Tian, J. Jia, J. Yang, H. Zhang, and T. Xu, "Progress and prospect of reliability assessment of power system with wind farm and energy storage system," *Smart Power*, vol. 47, no. 2, pp. 1–8, 2019.

[30] N. Zhang, L. Zhao, L. Guo, M. Zhang, X. Xu, J. Li, and W. Li, "Research on fast probabilistic production simulation algorithm for frequency response capacity planning," *Mod. Electr. Power*, vol. 40, no. 3, pp. 352–362, Jun. 2023.

[31] Q. Ma, L. Chen, L. Li, Y. Min, Y. Gong, and K. Liang, "Effect of grid-following VSC on terminal frequency," *IEEE Trans. Power Syst.*, vol. 38, no. 2, pp. 1775–1778, Mar. 2023.

[32] S. Engelken, C. Strafiel, and E. Quitmann, "Frequency measurement for inverter-based frequency control," in *Proc. 15th Int. Wind Integr. Workshop*, 2016, pp. 1–18.

[33] J. C. S. Sousa, O. R. Saavedra, and S. L. Lima, "Decision making in emergency operation for power transformers with regard to risks and interruptible load contracts," *IEEE Trans. Power Del.*, vol. 33, no. 4, pp. 1556–1564, Aug. 2018.

[34] H. Gu, R. Yan, and T. K. Saha, "Minimum synchronous inertia requirement of renewable power systems," *IEEE Trans. Power Syst.*, vol. 33, no. 2, pp. 1533–1543, Mar. 2018.

[35] "Task force code—System dynamic issues for the synchronous zone of continental Europe," RG-CE Syst. Protection Dyn. Sub Group, ENTSO-E, Sep. 2017.
[36] J. Liu, C. Wang, J. Zhao, and T. Bi, "RoCoF constrained unit commitment considering spatial difference in frequency dynamics," *IEEE Trans. Power Syst.*, vol. 39, no. 1, pp. 1–14, Jan. 2023.

NA ZHANG was born in Jinzhou, Liaoning, China, in 1986. She received the Ph.D. degree in electrical engineering from Dalian University of Technology, Dalian, China, in 2014. She is currently a Senior Engineer and the Vice Director of the Strategic Development Research Center, State Grid Liaoning Economic Research Institute. Her research interests include integrated energy system planning, clean energy absorption and application technology, and electric power market.

YONGRUI LI was born in 1984. He received the B.S. degree from Northeastern University, Shenyang, China, in 2006. He is currently the Vice Director of the Development Department, State Grid Liaoning Electric Power Supply Company Ltd. His research interests include power statistics and power system dispatch operations.

QILI DING (Student Member, IEEE) was born in 2001. He received the B.S. degree in electrical engineering from Dalian Maritime University (DMU), Dalian, China, in 2022. He is currently pursuing the M.S. degree with the School of Electrical Engineering, Dalian University of Technology (DUT), Dalian. His research interests include power system frequency stability analysis and control.

XINGGAN ZHANG was born in 2002. He is currently pursuing the B.S. degree in electrical engineering with Dalian University of Technology (DUT), Dalian, China, where he will go to pursue the M.S. degree with the School of Electrical Engineering. His research interests include power system frequency stability analysis and control.

HAIWEI JIANG was born in 1996. He received the B.S. degree in electrical engineering from Dalian Jiaotong University, Dalian, China, in 2018, and the M.S. degree in electrical engineering from North China Electric Power University, Beijing, China, in 2021. He is currently an Engineer with the State Grid Liaoning Economic Research Institute. His research interests include power system automation, with a recent focus on energy and electricity development plan.

WEIDONG LI (Member, IEEE) received the B.S. degree in electrical engineering from Xi'an Jiaotong University, in 1985, the M.S. degree in electrical engineering from Northeast Electric Power University, Jilin, China, in 1988, and the Ph.D. degree in electrical engineering from Harbin Institute of Technology, Harbin, China, in 1997. He is currently a Professor of electrical engineering with Dalian University of Technology (DUT), Dalian, China, where he was the Dean of the School of Electrical Engineering, from 2011 to 2016. His research interests include power system automation, with a recent focus on frequency stability analysis and control of new power systems.